2D Materials

PAPER • **OPEN ACCESS**

Enhancing catalytic epoxide ring-opening selectivity using surface-modified $Ti_3C_2T_x$ MXenes

2D Materials

PAPER

Enhancing catalytic epoxide ring-opening selectivity using surface-modified $Ti_3C_2T_x$ MXenes

Thierry K Slot[1], **Varun Natu**[2], **Enrique V Ramos-Fernandez**[3], **Antonio Sepúlveda-Escribano**[3], **Michel Barsoum**[2], **Gadi Rothenberg**[1] and **N Raveendran Shiju**[1,*]

[1] Van't Hoff Institute for Molecular Sciences, University of Amsterdam, Science Park 904, Amsterdam 1098XH, The Netherlands
[2] Material Science and Engineering, Drexel University, 3141 Chestnut Street, Philadelphia, PA, United States of America
[3] Laboratorio de Materiales Avanzados, Departamento de Química Inorgánica—Instituto Universitario de Materiales de Alicante, Universidad de Alicante, Alicante, Spain
[*] Author to whom any correspondence should be addressed.

E-mail: n.r.shiju@uva.nl

Keywords: heterogeneous catalysis, MXene, acid catalysis, epoxide ring opening, epoxide isomerisation, styrene oxide

Supplementary material for this article is available online

OPEN ACCESS

RECEIVED
26 October 2020

REVISED
18 January 2021

ACCEPTED FOR PUBLICATION
24 February 2021

PUBLISHED
19 March 2021

Abstract

MXenes are a new family of two-dimensional carbides and/or nitrides. Their 2D surfaces are typically terminated by O, OH and/or F atoms. Here we show that $Ti_3C_2T_x$—the most studied compound of the MXene family—is a good acid catalyst, thanks to the surface acid functionalities. We demonstrate this by applying $Ti_3C_2T_x$ in the epoxide ring-opening reaction of styrene oxide (SO) and its isomerization in the liquid phase. Modifying the MXene surface changes the catalytic activity and selectivity. By oxidizing the surface, we succeeded in controlling the type and number of acid sites and thereby improving the yield of the mono-alkylated product to >80%. Characterisation studies show that a thin oxide layer, which forms directly on the $Ti_3C_2T_x$ surface, is essential for catalysing the SO ring-opening. We hypothesize that two kinds of acid sites are responsible for this catalysis: In the MXene, strong acid sites (both Lewis and Brønsted) catalyse both the ring-opening and the isomerization reactions, while in the Mxene–TiO_2 composite weaker acid sites catalyse only the ring-opening reaction, increasing the selectivity to the mono-alkylated product.

1. Introduction

MXenes are getting increased attention as novel two-dimensional (2D) materials. They are prepared by delaminating MAX phases, which are atomically layered solids where M is an early transition metal, A is a group IIIA/IVA element, and X is carbon or nitrogen [1]. MXenes are denoted by $M_{n+1}X_nT_x$, where T stands for a terminating functional group that depends on the delamination conditions [2–5]. These materials are very versatile. They can be prepared from a variety of MAX phases, and their surface chemistry can be controlled by the conditions of etching and delamination [6–11]. Although stable at high temperatures under inert conditions [12], they are sensitive to oxidation [13–17]. However, this sensitivity can be controlled by edge-capping the MXene sheets using polyanionic salts [18].

Thanks to their good conductivity and tuneable surface chemistry, [19–22] MXenes are widely applied in electrochemistry, batteries, sensors, separation science and electrocatalysis [23]. However, in heterogeneous catalysis, they are less used [24]. MXenes were recently applied in water–gas shift reaction [25], dehydrogenation of propane and isobutene [26], nitrogen fixation [27], methane dehydroaromatisation [28], and oxidation reactions [29, 30]. As far as we know, these are the only published thermocatalytic applications.

As far as we know, MXenes have not been used for low-temperature, liquid-phase reactions and little is known about their function in such systems. Studying the effect of their surface functional groups in acid-catalysed reactions is especially interesting, as these groups might act as acid catalyst sites. In this work, we explore the $Ti_3C_2T_x$ MXene and its derivatives as

catalysts for acid-catalysed reactions using the styrene oxide (SO) ring opening reaction as a model reaction (equation (1)). This reaction is an important route to bifunctional compounds, such as β-alkoxy alcohols, which are precursors for a range of pharmaceuticals. To the best of our knowledge, MXenes have not been used as catalysts in this reaction. The SO ring opening is usually acid-catalysed, but can also be catalysed by a base [31–33]. The selectivity to the desired product depends on the catalyst [34–36]. Homogeneous and heterogeneous catalysts such as Lewis acids, Brønsted acids and mineral acids were used previously for the alcoholysis of epoxides. However, many of these catalysts are difficult to separate and recycle and some need harsh reaction conditions to reach high conversions [37–43]. By studying the reaction kinetics and mechanism, we show that the kinetics and selectivity in epoxide ring opening can be controlled and boosted by modifying the surface of $Ti_3C_2T_x$, which influences the number and type of acid sites. We further show that by oxidizing the MXene to form a $Ti_3C_2T_x$–TiO_2 composite the activity increases. The increase, however, depends on the presence of $Ti_3C_2T_x$ multilayers.

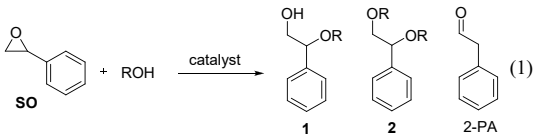

(1)

2. Experimental details

Detailed descriptions of the instrumentation and methods are included in the supporting information.

2.1. MXene ($Ti_3C_2T_x$) synthesis

The Ti_3AlC_2 powders were synthesized by mixing titanium carbide (Alfa Aesar, 99.5%), aluminium (Al) (Alfa Aesar, 99.5%, 325 mesh), and titanium (Alfa Aesar, 99.5%, 325mesh), powders in a molar ratio of 2:1.05:1, respectively. The mixture was ball milled at 100 rpm for 24 h (this step was used to just mix the powders and no particle size reduction or reaction happens here). The powders are then transferred to an alumina crucible and heated under flowing argon, Ar, at 1350 °C for 2 h. The heating and cooling rates were set at 5 °C min^{-1}. The resulting loosely sintered blocks were ground using a titanium nitride coated milling bit on a drill press. The milled powders were passed through a 400 mesh (particle size < 38 μm) sieve for further experiments.

To etch the Ti_3AlC_2 powder (1.0 g) it was added to 10 ml of 10% HF solution (figure 1). The mixture was stirred for 24 h at room temperature and 300 rpm. The resulting slurry was transferred into a 50 ml centrifuge tube and DI water was added to completely fill the remaining volume. It was then centrifuged at 3500 rpm for 2 min and the resulting clear supernatant was discarded. This washing was repeated several times until the pH of the solution was ≈7. After which the bottom sediment was collected and dried under vacuum before further testing. Catalysts were exposed to air for one week prior to use a reaction, to avoid induction periods at the beginning of the reaction.

2.2. Synthesis of MXene–TiO_2 composite

MXene (100 mg) was suspended in 20 ml water in a 75 ml autoclave with PTFE liner and a 30 × 8 mm stirring bar. The autoclave was sealed and quickly heated to 285 °C and kept at this temperature for 30 min while stirring at 800 rpm. Then, the reactor was allowed to cool down to room temperature. The material was washed (5×) with water and dried overnight under vacuum at 30 °C.

2.3. Catalytic testing

A stock solution of SO was prepared by dissolving SO (5 ml, 4.36 mmol) and bromobenzene (5 ml) in absolute ethanol to a total volume of 50 ml. The reactions were performed in 20 ml test tubes, sealed with a screw cap. SO stock solution (5 ml) was then added to 5.0 mg of the catalyst. Tubes were heated in an oil bath and stirred at 600 rpm. Aliquots of 120 μl were taken from the reaction mixture, diluted 10× with ethanol, filtered through a PTFE filter (0.45 μm) and analysed by gas chromatography, GC, (He carrier, HP-5 column).

2.4. Kinetic studies

Kinetic experiments were run in duplicate, in an oven-dried 100 ml three-neck flask equipped with a reflux condenser and a slight N_2 overpressure (<50 mbar). SO stock solution (20 ml) was added to 20 mg catalyst. All open necks were stoppered to avoid N_2 leakage. During the reaction, aliquots of 120 μl were taken from the reaction, diluted 10× with ethanol, filtered through a PTFE filter (0.45 μm) and analysed by GC.

2.5. Characterization

All chemicals were obtained from commercial sources (>97% pure) and used as received. GC was performed with a Perkin Elmer Clarus 500, equipped with a flame ionization detector and a 30 m Agilent polysiloxane HP-5 column (0.32 mm ID, 0.25 μm). He was used as carrier gas and the column oven was heated from 60 °C to 250 °C with a 25 °C min^{-1} heating rate and held at the final temperature for 5 min. Sample solution (1.0 μl) was injected using a split injector with a 1:50 split ratio.

Diffuse reflectance infrared Fourier transform spectroscopy (DRIFTS) was done on a FTIR (Nicolet 6700) spectrometer with a MCT detector (cooled

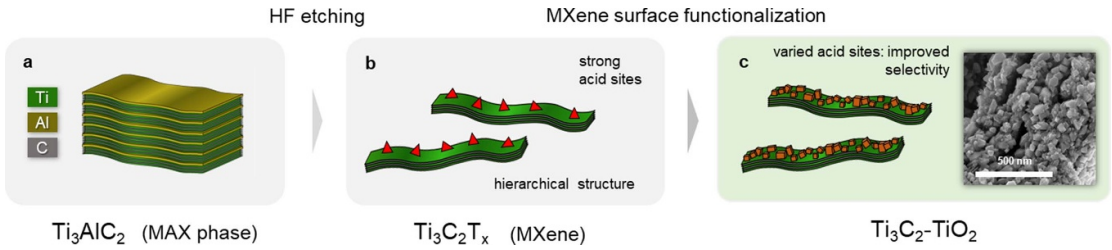

Figure 1. Cartoon illustrating the material synthesis from (a) MAX phase to (b) MXene, followed by (c) surface functionalisation creating Mxene–TiO_2 composites (inset: SEM image of the MXene–TiO_2 composite).

with liquid N_2). The DRIFTS sample cell (Praying Mantis, Harrick) was fitted with CaF_2 windows and a PID-controlled heater allowing samples to be heated to 700 °C. Samples were preheated in helium to 350 °C for 1 h, and then stepwise cooled till 25 °C while taking background spectra of the pre-heated sample at every sample temperature. A constant helium flow of 20 ml min^{-1} was maintained throughout the analysis. Spectra of adsorbed pyridine were collected after treating the pre-heated sample in a flow of 1.0–1.4 vol.% pyridine in He for 10 min, followed by evacuation by an oil pump for 30 min. All spectra were measured at their respective temperatures with resolution of 4 cm^{-1} and accumulation of 64 scans. Confocal Raman spectra were recorded at 532 nm using a Renishaw (Wottonunder-Edge, United Kingdom) InVia Reflex Raman microscope with a 532 nm frequency-doubled Nd:YAG excitation source in combination with an 1800 lines mm^{-1} grating, and a Peltier-cooled CCD detector (203 K). The instrument included a Leica light microscope with a 50× air objective. The 521 cm^{-1} Raman shift of an internal silicon standard was used to verify the spectral calibration of the system. X-ray photoelectron spectroscopy (XPS) analysis was carried out in a K-Alpha Spectrometer (Thermo-Scientific). The assignment of the C 1s binding energies was done according to the criteria used by Ganguly *et al* 284.5 eV for C=C (aromatic double bonds), 285.5 eV for C–OH and sp^3 C–C, 286.5 eV for epoxy, 287.5 for sp^2 C=O (carbonyls, lactones) and 289 eV for carboxylic groups [44]. X-ray diffraction (XRD) measurements were carried out on a Rigaku Miniflex x-ray diffractometer from 4° to 70° using a 2.0° min^{-1} scan rate.

Scanning electron microscope images were taken on a FEI Verios 460 instrument using a 5 kV accelerating voltage. HRTEM images were recorded on a FEI Tecnai G2 F20 S-Twin high-resolution transmission electron microscope, TEM, working at 200 kV (point resolution: 0.24 nm, lattice resolution 0.102 nm, information resolution 0.14 nm). STEM-EDS images were recorded using an energy dispersive spectroscope, EDS, detector with energy resolution <127 eV and a resolution of 0.20 nm.

3. Results and discussion

First, we prepared $Ti_3C_2T_x$ MXenes by etching Ti_3AlC_2 powders with 10% HF for 24 h under continuous stirring (figure 1). Rinsing and washing gave a multi-layered MXene with –OH, –O and –F as its main surface functional groups. Recent studies suggest that MXenes' sensitivity to oxidation can be used to create materials with new structural and electronic properties [14, 45, 46]. We envisaged that such treatments could enhance or block certain reaction pathways by altering the surface structure, giving us control over reactivity and selectivity. One such treatment consists of exposing $Ti_3C_2T_x$ to water at hydrothermal conditions. For this, we treated the MXene in autoclave at 285 °C for 30 min. Then, the reactor was quenched in water and the material was washed with water and dried under vacuum at 30 °C for 12 h. This grows small crystals of TiO_2 on the MXene surface, while leaving the bulk of the MXene layers intact. XRD analysis (figure S1 (available online at stacks.iop.org/2DM/8/035003/mmedia)) revealed that these crystals have both rutile (27°, 38° and 55°) and anatase (25° and 48°) phases in a ratio 1:2–1:3 [47]. These appear as a range of unordered crystals sticking out of the $Ti_3C_2T_x$ basal planes, as shown by scanning electron microscopy (figure 2). Compared to low-temperature air oxidation methods, our hydrothermal method produces a mix of rutile and anatase titania, possibly utilizing structural defects in the MXene surface to initiate crystallization [48–50]. Raman spectroscopy showed that the surface consists of anatase titania on both the MXene and the $Ti_3C_2T_x$–TiO_2 composite (figure S2).

We then compared Ti_3AlC_2 and its MXene, $Ti_3C_2T_x$, in the catalytic ring opening of SO by methanol. The MAX phase showed low activity and selectivity to the mono-alkylated product **1** (table 1, entry 2 and 8). Conversely, a MXene made from this MAX phase showed a high conversion (98%) and selectivity (90%) to product **1** in 2.5 h. This shows that etching out the Al layers increases the catalytic activity. We also ran a set of control experiments using MXenes stored under both argon and air to see the

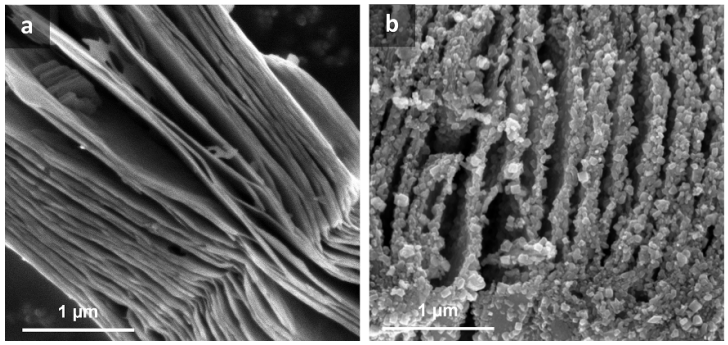

Figure 2. SEM micrographs of (a) $Ti_3C_2T_x$ multilayers, and (b) $Ti_3C_2T_x$–TiO_2 composite showing TiO_2 particles at the multilayer edges.

Table 1. Catalytic results for the styrene oxide ring opening by methanol[a].

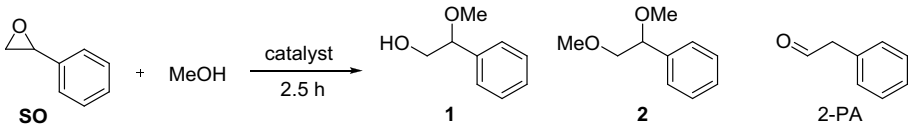

#	T (°C)	Catalyst	Conversion	Selectivity[b]		
				1 (%)	**2** (%)	**2-PA** (%)
1	60	No catalyst[c]	1	—	—	—
2	60	Ti_3AlC_2	15	22	15	63
3	60	Ti_3AlC_2, H_2O_2 treated	17	41	3	54
4	60	Ti_3C_2, under Ar[c]	75	36	3	51
5	60	Ti_3C_2, air exposed[c]	98	73	18	9
6	60	Graphene oxide[d]	43	42	53	2
7	80	No catalyst[c]	7	—	—	—
8	80	Ti_3AlC_2	25	51	22	27
9	80	Ti_3AlC_2, H_2O_2 treated	31	70	1	28
10	80	Ti_3C_2, under Ar[c]	98	90	6	4
11	80	Ti_3C_2, air exposed[c]	> 99	88	5	5
12	80	Graphene oxide[d]	94	53	46	10

[a] Reaction conditions: 0.5 ml styrene oxide and 5 mg of catalyst in 5 ml methanol in a closed container; stirred for 2.5 h.
[b] Selectivity towards the single product, based on GC analysis (PhBr, 100 μl internal standard).
[c] Average of duplicate experiments.
[d] Prepared by Hummers method.

influence of surface oxidation/hydration [13]. The sample stored under argon showed a short induction period (15 min) before product **1** appeared. After this, the reaction proceeded quickly, whereas the air-exposed sample performed well from the beginning (cf. table 1, entries 4/5 and 10/11).

Subsequently, we tested the pristine and composite MXene materials in the SO ring opening reaction (figure 3). A series of control experiments (data not shown) showed that the reactivity of ethanol was comparable to that of methanol, so we switched to ethanol for safety reasons. Products **1** and **2** were identified and characterized using ^{1}H NMR and two-dimensional ^{1}H–^{1}H correlation spectroscopy (COSY, see figures S7 and S8). Product **1** is easily distinguished by its characteristic spin splitting in the C$\underline{H}_2$C$\underline{H}$–O$\underline{H}$ system in ^{1}H NMR. Chromatography analysis showed the formation of an intermediate, 2-phenyl acetaldehyde (2-PA). The isomerization of SO to 2-PA over $Ti_3C_2T_x$ is very fast, taking only minutes at 45 °C (figure 3(a)). The 2-PA is then converted into product **2** following first order kinetics (figure S3). Interestingly, the kinetics of the reaction in the presence of the structurally altered

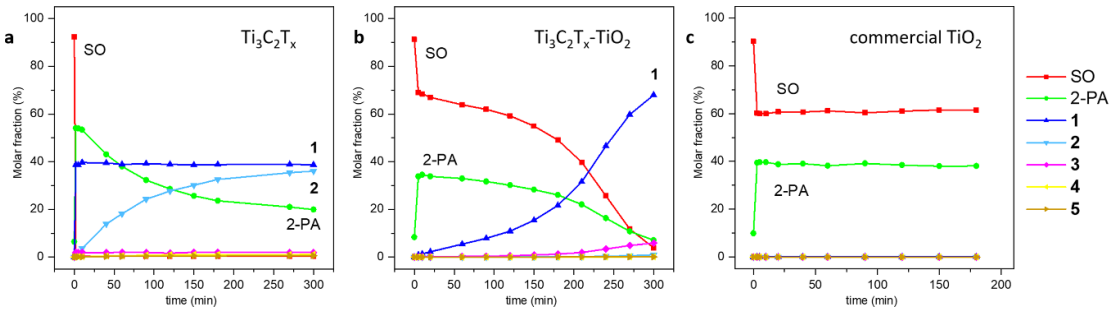

Figure 3. Styrene oxide reaction with (a) pristine $Ti_3C_2T_x$ MXene, (b) oxidized $Ti_3C_2T_x$ with TiO_2 crystals on its surface, and (c) a control reaction with TiO_2. Molar fractions of compounds were determined by GC using PhBr as an internal standard. SO = styrene oxide, 2-PA = 2-phenyl acetaldehyde, and **1**–**5** are reaction products. Reaction temperature was 45 °C.

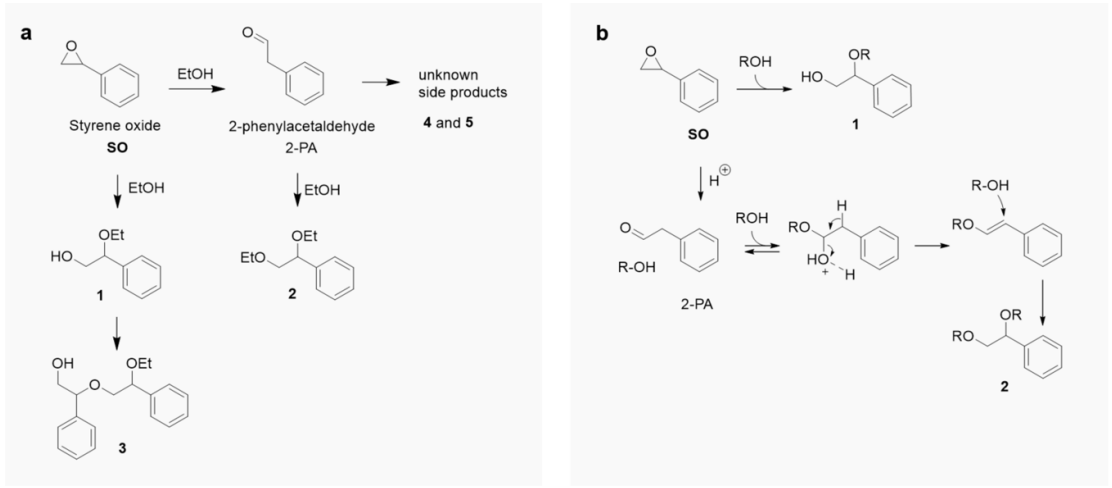

Scheme 1. (a) Reaction pathways, products and by-products in the ring opening of styrene oxide catalysed by $Ti_3C_2T_x$ and $Ti_3C_2T_x$–TiO_2 composite. (b) Reaction mechanism from 2-PA into products **1** and **2**.

MXene—the $Ti_3C_2T_x$–TiO_2 composite were totally different compared with the non-treated $Ti_3C_2T_x$ flakes (figure 3(b)). The reaction starts rapidly, and the remainder of the SO was converted to product **1** with a small amount of product **2**. This shows that the surface treatment can limit the conversion of SO into 2-PA, allowing the formation of product **1** in high yields. Since the treatment introduces titania crystals on the surface, the reactivity change may be caused by these crystals. To check this, we ran a control using a commercial titania (Degussa P25, anatase:rutile ratio ~3:1). However, this yielded only 2-PA and no other products (cf. figure 3(c)), showing that TiO_2 is not solely responsible for the reactivity of the treated MXene.

With bulk TiO_2 as catalyst, the concentration of SO decreases steeply. However, the reaction stops within 1–2 min. Control experiments confirmed that SO and 2-PA are not in equilibrium: neither catalyst yielded any SO when starting from 2-PA as substrate (figure S4). Using 2-PA as starting material we could also verify that 2-PA is the intermediate towards product **2**. Scheme 1(a) gives an overview of the reaction pathways. Regarding the steep drop in SO in the first few minutes of the reaction, we hypothesize that the isomerization of SO initiates polymerization around the stronger acid sites, blocking them from further action. The $Ti_3C_2T_x$–TiO_2 catalyst has fewer strong acid sites, resulting in a smaller concentration drop of SO. XPS analysis (figure 4, blue curve) of the spent catalyst shows an increase in the signal at 286.3 eV, corresponding to organic CH_x or CO residues at the expense of C–Ti–T_x at 281.9 eV, (figure 4, green curve). This supports our hypothesis of organic residues deposited on the C–Ti–F bonds that are reactive towards nucleophilic attack. A similar, but less pronounced, increase in CH_x peak intensities was observed for the $Ti_3C_2T_x$–TiO_2 composite after reaction (figure S5, C 1s).

We tested several alcohols as solvent/reactant for the reaction with SO (table 2). Methanol and ethanol gave good conversions (>99%) and were selective towards product **1**. Isopropyl alcohol gave equal amounts of **1** and **2**, while *t*-BuOH gave mainly product **2**. This can be explained by a examining the reaction mechanisms of SO and 2-PA with alcohols (scheme 1(b)). Bulkier alcohols such as *t*-BuOH react slower towards **1**, because the alcohol attacks a

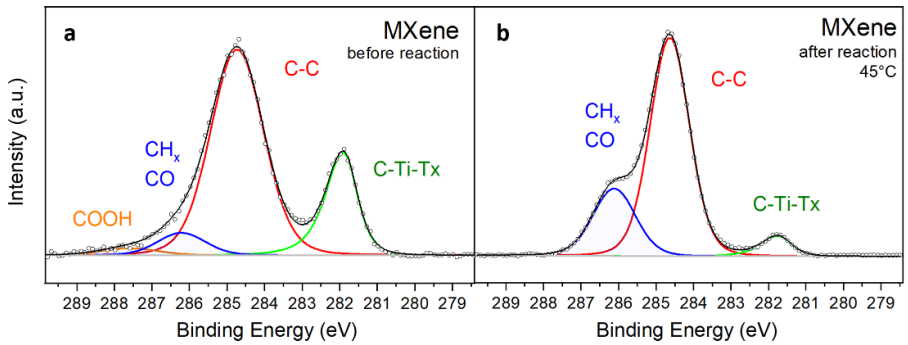

Figure 4. XP spectra of the C 1s region of $Ti_3C_2T_x$, (a) before and (b) after reaction. The peaks are deconvoluted as shown.

Table 2. Epoxide ring opening catalysed by Ti_3C_2 in different solvents[a].

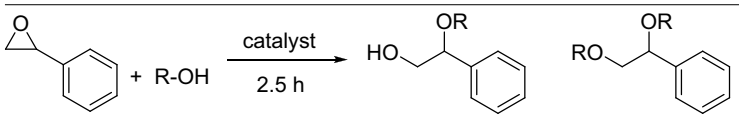

SO 1 2

Entry	Substrate	Conversion[b] (%)	Selectivity[c] **1** (%)	**2** (%)	**2-PA** (%)
1	Methanol	>99 (5)	73	18	9
2	Ethanol	>99 (1)	50	46	4
3	Isopropanol	99 (0)	35	35	24
4[d]	*tert*-butanol	79 (0)	4	23	68

[a] Reaction conditions: epoxide (0.874 mmol) and $Ti_3C_2T_x$ (1.0 mg) in 1 ml ethanol; stirred at 60 °C for 2.5 h.
[b] Conversion of both reactions with and without catalyst (without catalyst in parenthesis).
[c] Selectivity towards the single product, based on GC analysis (PhBr as internal standard).
[d] An undetermined by-product, <3%, was also observed.

sterically hindered position. Yet isomerization of SO into 2-PA still takes place at a normal rate, consuming the SO before significant amounts of **1** can form. This gives more 2-PA, which converts to product **2** as follows: first, it forms a hemiacetal with one alcohol molecule. This dehydrates, yielding a double bond, which can be attacked at the benzylic carbon. Overall, the reduced rate towards **1**, and the increased concentration of 2-PA, lead to a higher selectivity to product **2** with bulkier alcohols. The $Ti_3C_2T_x$ MXene gives a TOF of 55 h^{-1} for the reaction with methanol at 60 °C. It outperforms other titanium-based solid catalysts (cf. Ti-MCM-41 with a TOF of 29 h^{-1}, and a lower yield of product **1** [51]). Polymers with sulfonic acid groups (such as Amberlyst) generally have better performance, but they swell and are generally less stable at higher temperatures [52].

We then tested the catalytic activity of MXene for ethanolysis of other epoxides (table 3). The simple unhindered epoxides (entries 1–5) react readily giving high conversion (>99%) at high selectivity (89%) against a background reaction of <1% conversion, showing that MXene catalysis has a broad scope for epoxide ring-opening reactions. Sterically hindered epoxides (entries 6 and 7) gave lower conversion, but this was expected as both *i*-Pr and *t*-Bu groups are quite bulky. A primary alcohol group improved conversion and selectivity (*cf* entries 4 and 5), likely because of its electron-withdrawing nature.

The fact that both isomerization and epoxide ring opening are acid-catalysed suggests that both $Ti_3C_2T_x$ and the $Ti_3C_2T_x$–TiO_2 composite have acid sites. We envisage two kinds of acid sites: strong sites (present on MXene) catalysing both the reaction of SO to 2-PA and product **1**, and weaker ones, present on $Ti_3C_2T_x$–TiO_2, that only catalyse the ring opening of SO to give product **1**. In short, we propose that the hydrothermal treatment blocks most of the strong acid sites, leaving only the weaker acid sites to catalyse the reaction.

Characterizing the acid sites is challenging. Ammonia temperature-programmed desorption did not show significant desorption. Pyridine DRIFTS reveals the presence of both Lewis and Brønsted acid sites on $Ti_3C_2T_x$ (figure 5(c)). The bands at 1450, 1588, 1612 cm^{-1} are commonly assigned to Lewis acid sites, the one at 1545 cm^{-1} to Brønsted acid sites and the one at 1486 cm^{-1} to a combination of Lewis and Brønsted acid sites [53–56]. The broad signal at 1425 cm^{-1} is assigned to H-bonded pyridine. However, because of the low signal we could not quantify the Lewis/Brønsted site

Table 3. Epoxide ring opening of different epoxides by Ti_3C_2 in ethanol[a].

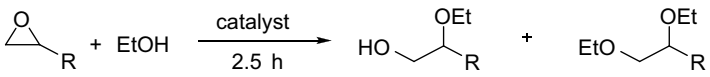

Entry	Substrate	Conversion[b] (%)	Selectivity[c] (%)	Background conversion[e]
1	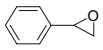	> 99	89	1
2		> 99	96	0
3		99	95	0
4		79	74	3
5[d]		33	53	3
6		2	76	0
7		6	98	4

[a] Reaction conditions: epoxide (0.874 mmol) and Ti_3C_2 (1.0 mg) in 1 ml ethanol; stirred at 80 °C for 2.5 h.
[b] Conversion of both reaction with (top) and without catalyst (bottom).
[c] Selectivity towards the single product, based on GC analysis (PhBr as internal standard).
[d] An undetermined by-product was observed.
[e] Background reaction with same conditions, yet leaving out the catalyst.

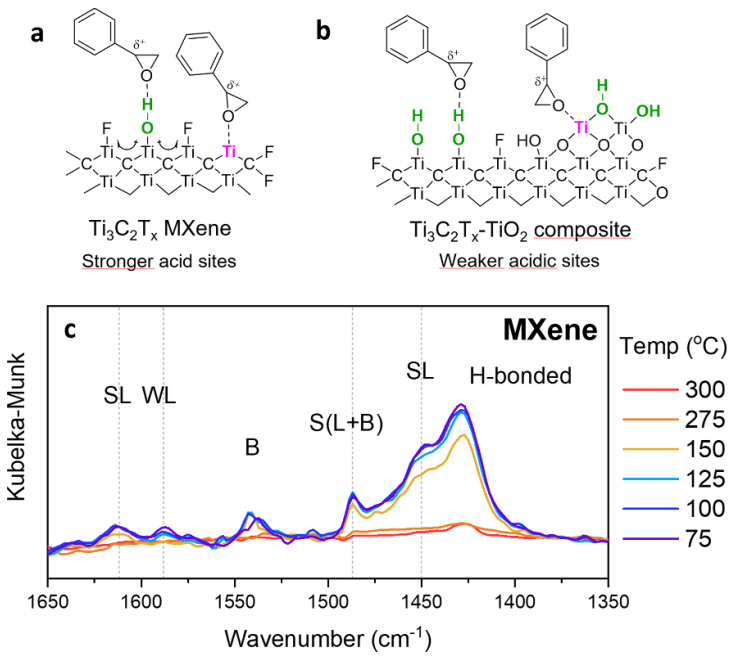

Figure 5. Illustration of types of acid sites on $Ti_3C_2T_x$ (top) showing (a) stronger sites close to F-groups, and (b) weaker sites from O–Ti bonds. (c) Pyridine DRIFTS for the $Ti_3C_2T_x$ sample. S: strong, W: weak, L: Lewis acid, B: Brønsted acid. For example: WL = weak Lewis acid.

ratios. Similarly, the signal-to-noise ratio of pyridine DRIFTS of the $Ti_3C_2T_x$–TiO_2 composites was too low to assign the type of acid sites. This shows that the $Ti_3C_2T_x$–TiO_2 composite has fewer acid sites than $Ti_3C_2T_x$. The latter's surfaces are functionalized by –OH, –O and –F [45]. XPS revealed a small amount of moderately acidic carboxylic groups had formed after hydrothermal treatment (C 1s, figure 6). Additionally, a lot of TiO_2 had formed on the surface at the expense of C–Ti–T_x groups (Ti 2p, O 1s, and C 1s, figure 6). Our hypothesis is that the fluorinated MXene surface is responsible for the strongest acid sites (figure 5(a)). Lewis acidity is derived from Ti^+ sites and Brønsted acidity is caused by surface –OH groups adjacent to –F groups. The –F groups withdraw electron density from the –OH groups making them even more acidic. In the composite, most of the surface is covered with TiO_2 crystals with known Lewis and Brønsted acidity (figure 5(b)) [57]. The Ti 2p spectrum after reaction (figure S6) showed a decrease in Ti–C contributions and an increase in Ti–O contributions. This suggests the surface is being

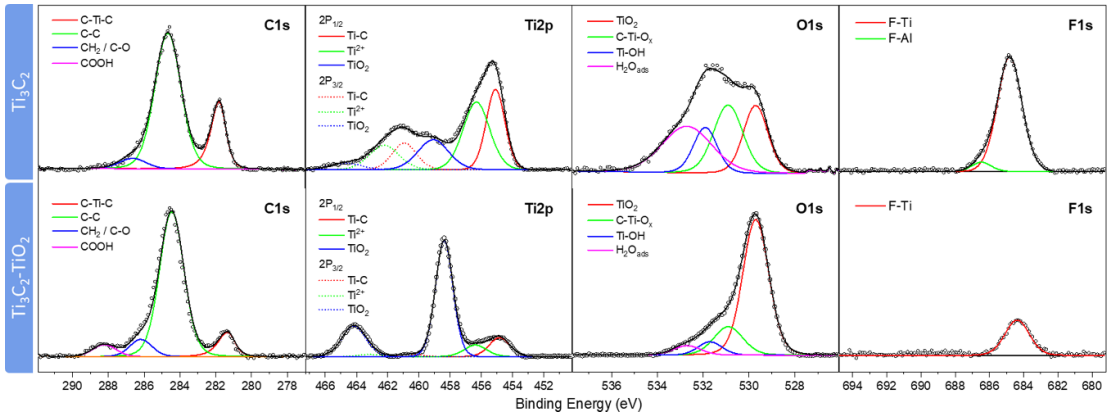

Figure 6. Normalized XPS spectra of $Ti_3C_2T_x$ (top) and $Ti_3C_2T_x$–TiO_2 composite (bottom). Intensity is in arbitrary units.

slowly oxidized into TiO_2 during the reaction. Similarly, the O 1s showed an increase in signals at 531.5 eV and 532.8 eV, corresponding to C–Ti–O_x and Ti(OH)$_x$, moieties, respectively. TEM analysis (figure S7) revealed a thin layer (<5 nm) of amorphous titania forming at the surface during the reaction. The F 1 s spectrum did not show any new contributions, albeit that the total F signal decreased after reaction (figure S6).

Similar changes occurred during reaction of the composite, though less pronounced (figure S5). The C 1s spectrum showed an increase in alkyl contributions and a decrease of fluorine contributions. O 1s showed an increase in Ti^{2+}–O and hydrated Ti(OH)$_x$ contributions. Ti(OH)$_x$ groups are the major contributors to the Lewis/Brønsted acidity [58, 59]. The increase in reactivity after 150 min (figure 3(b)) is likely related to this increase.

4. Conclusion

$Ti_3C_2T_x$ flakes can be used as acid catalysts for isomerization and ring opening of SO. These two reactions compete on the $Ti_3C_2T_x$ surfaces, likely because of the strong acid sites, promoted by the F-groups. The presence of small TiO_2 crystals at the $Ti_3C_2T_x$ flake edges produced by a hydrothermal treatment in H_2O, containing both Brønsted and Lewis acid sites, is responsible for the acid catalysis. The hydrothermal treatment creates a TiO_2 layer that blocks most of the strong acid sites responsible for the isomerization reaction. This alters the reaction kinetics, increasing the selectivity of the main product **1** up to 90%. This opens doors to apply MXenes and/or their composites in other acid-catalysed reactions as well. Overall, the availability of many different types of MXenes and their derivatives offers a new opportunity for controlling selectivity and activity in catalysis.

Acknowledgments

We thank D. Smit and M. Hanson for help with the kinetic studies. TKS was supported by the NWO TOP-PUNT *Catalysis in Confined Spaces* (Grant 718.015.004). EVRF and ASE acknowledge financial support by MINECO (Spain) through the projects MAT2017-86992-R and MAT2016-80285-P. VN and MWB thank NSF DMR 1740795 for financial support.

ORCID iDs

Gadi Rothenberg https://orcid.org/0000-0003-1286-4474
N Raveendran Shiju https://orcid.org/0000-0001-7943-5864

References

[1] Barsoum M W 2013 *MAX Phases: Properties of Machinable Ternary Carbides and Nitrides* (Weinheim: Wiley-VCH Verlag GmbH & Co. KGaA)
[2] Naguib M, Mochalin V N, Barsoum M W and Gogotsi Y 2014 *Adv. Mater.* **26** 992–1005
[3] Ronda-Lloret M, Marakatti V S, Sloof W G, Delgado J J, Sepúlveda-Escribano A, Ramos-Fernandez E V, Rothenberg G and Shiju N R 2020 *ChemSusChem* **13** 6401–8
[4] Hart J L, Hantanasirisakul K, Lang A C, Anasori B, Pinto D, Pivak Y, van Omme J T, May S J, Gogotsi Y and Taheri M L 2019 *Nat. Commun.* **10** 522
[5] Gao G, O'Mullane A P and Du A 2017 *ACS Catal* **7** 494–500
[6] Persson Per O Å and Rosen J 2019 *Curr. Opin. Solid State Mater. Sci.* **23** 100774
[7] Fredrickson K D, Anasori B, Seh Z W, Gogotsi Y and Vojvodic A 2016 *J. Phys. Chem.* C **120** 28432–40
[8] Handoko A D, Fredrickson K D, Anasori B, Convey K W, Johnson L R, Gogotsi Y, Vojvodic A and Seh Z W 2018 *ACS Appl. Energy Mater.* **1** 173–80
[9] Mashtalir O, Naguib M, Mochalin V N, Dall'Agnese Y, Heon M, Barsoum M W and Gogotsi Y 2013 *Nat. Commun.* **4** 1716
[10] Qian A, Seo J Y, Shi H, Lee J Y and Chung C-H 2018 *ChemSusChem* **11** 3719–23

[11] Anasori B, Lukatskaya M R and Gogotsi Y 2017 *Nat. Rev. Mater.* **2** 16098
[12] Seredych M, Shuck C E, Pinto D, Alhabeb M, Precetti E, Deysher G, Anasori B, Kurra N and Gogotsi Y 2019 *Chem. Mater.* **31** 3324–32
[13] Chae Y, Joon Kim S, Cho S-Y, Choi J, Maleski K, Lee B-J, Jung H-T, Gogotsi Y, Lee Y and Won Ahn C 2019 *Nanoscale* **11** 8387–93
[14] Tang H, Zhuang S, Bao Z, Lao C and Mei Y 2016 *ChemElectroChem* **3** 871–6
[15] Cao M, Wang F, Wang L, Wu W, Lv W and Zhu J 2017 *J. Electrochem. Soc.* **164** A3933
[16] Lotfi R, Naguib M, Yilmaz D E, Nanda J and van Duin A C T 2018 *J. Mater. Chem.* A **6** 12733–43
[17] Slot T K, Yue F, Xu H, Ramos-Fernandez E V, Sepúlveda-Escribano A, Sofer Z, Rothenberg G and Shiju N R 2020 *2D Mater.* **8** 015001
[18] Natu V, Hart J L, Sokol M, Chiang H, Taheri M L and Barsoum M W 2019 *Angew. Chem., Int. Ed.* **58** 12655–60
[19] Wang D, Li F, Lian R, Xu J, Kan D, Liu Y, Chen G, Gogotsi Y and Yingjin W 2019 *ACS Nano* **13** 11078–86
[20] Le T A, Bui Q V, Tran N Q, Cho Y, Hong Y, Kawazoe Y and Hyoyoung L 2019 *ACS Sustain. Chem. Eng.* **7** 16879–88
[21] Huang B, Li N, Ong W-J and Naigen Z 2019 *J. Mater. Chem. Mater. Energy Sustain.* **7** 27620–31
[22] Zhang J, Zhao Y, Guo X, Chen C, Dong C-L, Liu R-S, Han C-P, Li Y, Gogotsi Y and Wang G 2018 *Nat. Catal.* **1** 985–92
[23] Gogotsi Y and Anasori B 2019 *ACS Nano* **13** 8491–4
[24] Li Z and Wu Y 2019 *Small* **15** 1804736
[25] Deeva E B, Kurlov A, Abdala P M, Lebedev D, Kim S M, Gordon C P, Tsoukalou A, Fedorov A and Müller C R 2019 *Chem. Mater.* **31** 4505–13
[26] Li Z *et al* 2018 *Nat. Commun.* **9** 1–8
[27] Gouveia J D, Morales-García Á, Viñes F, Gomes J R B and Illas F 2020 *ACS Catal.* **10** 5049–56
[28] Thakur R, Hoffman M, Vahid Mohammadi A, Smith J, Chi M, Tatarchuk B, Beidaghi M and Carrero C A 2020 *ChemCatChem* **12** 3598–792
[29] Ding M, Chen W, Xu H, Shen Z, Lin T, Hu K, Lu C H and Xie Z 2020 *J. Hazard. Mater.* **382** 121064
[30] Ding M, Chen W, Xu H, Shen Z, Lin T, Hu K, Kong Q, Yang G and Xie Z 2019 *Chem. Eng. J.* **378** 122177
[31] Xue Z, Jiang J, Ma M-G, Li M-F and Mu T 2017 *ACS Sustain. Chem. Eng.* **5** 2623–31
[32] Santiago-Portillo A, Navalón S, Concepción P, Álvaro M and García H 2017 *ChemCatChem* **9** 2506–11
[33] Beletskiy E V, Hou X, Shen Z, Gallagher J R, Miller J T, Wu Y, Li T, Kung M C and Kung H H 2016 *J. Am. Chem. Soc.* **138** 4294–7
[34] Mirza-Aghayan M, Alizadeh M, Molaee Tavana M and Boukherroub R 2014 *Tetrahedron Lett.* **55** 6694–7
[35] Das A, Anbu N, Sk M, Dhakshinamoorthy A and Biswas S 2020 *ChemCatChem* **12** 1789–98
[36] Dutta P, Kalita P and Baruah P K 2016 *ChemistrySelect* **1** 1650–7
[37] Firouzabadi H, Iranpoor N, Jafari A A and Makarem S 2006 *J. Mol. Catal. Chem.* **250** 237–42
[38] Zaccheria F, Santoro F, Psaro R and Ravasio N 2011 *Green Chem.* **13** 545–8
[39] Nakhate A V and Yadav G D 2018 *ChemistrySelect* **3** 4547–56
[40] Matos I, Neves P D, Castanheiro J E, Perez-Mayoral E, Martin-Aranda R, Duran-Valle C, Vital J, Botelho Do Rego A M and Fonseca I M 2012 *Appl. Catal. Gen.* **439–440** 24–30
[41] Nogueira L S, Neves P, Gomes A C, Valente A A, Pillinger M and Gonçalves I S 2017 *J. Organomet. Chem.* **846** 185–92
[42] Bruno S M, Gomes A C, Abrantes M, Valente A A, Pillinger M and Gonçalves I S 2015 *J. Organomet. Chem.* **799–800** 179–83
[43] Mendes R F, Antunes M M, Silva P, Barbosa P, Figueiredo F, Linden A, Rocha J, Valente A A and Almeida Paz F A 2016 *Chem. Eur. J.* **22** 13136–46
[44] Ramos-Fernandez G, Muñoz M, García-Quesada J C, Rodriguez-Pastor I and Martin-Gullon I 2018 *Polym. Compos.* **39** 2116–24
[45] Ahmed B, Anjum D H, Hedhili M N, Gogotsi Y and Alshareef H N 2016 *Nanoscale* **8** 7580–7
[46] Zou H, He B, Kuang P, Yu J and Fan K 2018 *ACS Appl. Mater. Interfaces* **10** 22311–9
[47] Hernandez-Mejia C, Gnanakumar E S, Olivos-Suarez A, Gascon J J, Greer H F, Zhou W, Rothenberg G and Shiju N R 2016 *Catal. Sci. Technol* **6** 577–82
[48] Li Z, Wang L, Sun D, Zhang Y, Liu B, Hu Q and Zhou A 2015 *Mater. Sci. Eng.* B **191** 33–40
[49] Habib T, Zhao X, Shah S A, Chen Y, Sun W, An H, Lutkenhaus J L, Radovic M and Green M J 2019 *npj 2D Mater. Appl.* **3** 1–6
[50] Ghassemi H, Harlow W, Mashtalir O, Beidaghi M, Lukatskaya R, Gogotsi Y and Taheri L 2014 *J. Mater. Chem.* A **2** 14339–43
[51] Saikia L, Satyarthi J, Srinivas D and Ratnasamy P 2007 *J. Catal.* **252** 148–60
[52] Liu Y-H, Liu Q-S and Zhang Z-H 2008 *J. Mol. Catal. Chem.* **296** 42–46
[53] Lu J, Kosuda K M, van Duyne R P and Stair P C 2009 *J. Phys. Chem.* C **113** 12412–8
[54] Teles C A, de Souza P M, Rabelo-Neto R C, Griffin M B, Mukarakate C, Orton K A, Resasco D E and Noronha F B 2018 *Appl. Catal.* B **238** 38–50
[55] Wang Y H, Gao W G, Wang H, Zheng Y E, Na W and Li K Z 2017 *RSC Adv.* **7** 8709–17
[56] Osman A I, Abu-Dahrieh J K, Abdelkader A, Hassan N M, Laffir F, McLaren M and Rooney D 2017 *J. Phys. Chem.* C **121** 25018–32
[57] Ramos-Fernandez E V, Geels N J, Shiju N R and Rothenberg G 2014 *Green Chem.* **16** 3358–63
[58] Oi L E, Choo M-Y, Lee H V, Ong H C, Hamid S B A and Juan J C 2016 *RSC Adv.* **6** 108741–54
[59] Ropero-Vega J L, Aldana-Pérez A, Gómez R and Niño-Gómez M E 2010 *Appl. Catal. Gen.* **379** 24–9